Available online at www.sciencedirect.com
ScienceDirect
Journal of Solid State Chemistry 179 (2006) 3196–3208
JOURNAL OF SOLID STATE CHEMISTRY
www.elsevier.com/locate/jssc

Synthesis and characterization of hollandite-type material intended for the specific containment of radioactive cesium

A.Y. Leinekugel-le-Cocq[a], P. Deniard[a,*], S. Jobic[a], R. Cerny[b], F. Bart[c], H. Emerich[d]

[a]*Institut des Matériaux Jean Rouxel, Laboratoire de Chimie des Solides, 2 rue de la Houssinière, BP32229, 44322 Nantes cedex 3, France*
[b]*Laboratoire de Cristallographie, 24, quai Ernest-Ansermet, CH-1211 Geneva 4, Switzerland*
[c]*CEA Valrho Marcoule, DEN–DTCD–SECM, Laboratoire d'Etude des Matériaux Céramiques pour le Conditionnement, BP 17171, 30207 Bagnols sur Ceze cedex, France*
[d]*ESRF—SNBL, 6 rue Jules Horomitz, 38000 Grenoble, France*

Received 13 March 2006; received in revised form 15 May 2006; accepted 20 May 2006
Available online 13 June 2006

Abstract

The hollandite $Ba_1Cs_{0.28}Fe_{0.82}Al_{1.46}Ti_{5.72}O_{16}$, which has been proposed for the cesium-specific conditioning, can be synthesized either by an alcoxyde or a dry route. In both cases, a two-step protocol is applied, i.e., a calcination at 1000 °C followed by a sintering at 1200 °C. After sintering, both synthetic processes lead to a tetragonal form. According to the X-ray diffraction (XRD) patterns collected at the barium and the cesium *K* absorption edges, the different positions of these two elements have been evidenced with a more centered position in the oxygen cubic site of the tunnel for Ba than for Cs. On the contrary, after calcination, the two synthetic routes yield different products. The alcoxyde route gives rise to a mixture of the aforementioned Cs- and Ba-containing tetragonal *I*4/*m* hollandite, a Cs-only-containing monoclinic *I*2/*m* hollandite and an unidentified phase with a weak coherence length containing only Ba. The dry route yields a single tetragonal hollandite material containing Ba and Cs slightly different in composition from the targeted compound.

Keywords: Nuclear waste; Hollandite structure; X-ray diffraction; Rietveld refinement; Resonant XRD; Symmetry distortion

1. Introduction

Nowadays, nuclear energy ranks for approximately 17% of the total world production of electricity. In the 2020 horizon, based on the World Energy Council (WEC) estimates, this rate should be increased by 60% compared to 2000. In this framework, the problem of the recycling or confinement of cesium has to be addressed. Cesium is one of the principal radionuclides ensuing from the fission of uranium and is one of the most difficult to immobilize because of the high calorific power of ^{134}Cs (13.18 W/g with $T_{1/2} = 2.06$ years) and ^{137}Cs (0.417 W/g with $T_{1/2} = 30$ years), the long lifetime of ^{135}Cs (2.3×10^6 years), its volatility at high temperature and its tendency to form water soluble compounds. In the world, due to the nuclear activity, 11.09 kg of ^{135}Cs and 34.85 kg of ^{137}Cs were produced per day in 1995, that represents approximately 16.8 tons of radioactive cesium produced per year. In the particular case of France, where the nuclear power is the principal source of electricity (about 70% of the electrical production), the generation of radioactive cesium reaches 2.9 tons per year.

So far, different recycling treatments have been envisioned, within the framework of the law of December 30, 1991 in France [1], to take care of long lived elements: the transmutation and the specific conditioning.

Practically, transmutation of Cs appears unrealistic without any preliminary isotopic separation. In fact, according to Scheme 1, the isotopes ^{133}Cs (stable) and ^{134}Cs ($T_{1/2} = 2.06$ years) will increase to a significant degree the assessment in ^{135}Cs ($T_{1/2} = 2.3.10^6$ years) during the neutron irradiations because of their high neutron absorption capability compared to that of ^{135}Cs [2].

The second solution, specific conditioning, was oriented on materials for the specific immobilization of radioactive

*Corresponding author. Fax: +33 2 40 37 39 95.
E-mail address: philippe.deniard@cnrs-imn.fr (P. Deniard).

0022-4596/$ - see front matter © 2006 Elsevier Inc. All rights reserved.
doi:10.1016/j.jssc.2006.05.047

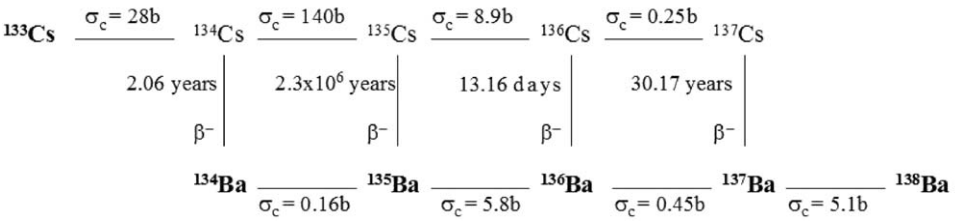

Scheme 1. Cesium evolution under neutron irradiation.

cesium after its separation from the High Level radioactive liquid Wastes (HLW) with calixarenes complexes [3].

For this purpose, a hollandite ceramic was envisaged because of previous investigations on the so-called Synroc (SYNthetic ROCk) (multiphase titanate ceramic), samples consisting of a mixture of perovskite, zirconolite, titanium oxide and hollandite. This synthetic mineral was originally developed for the immobilization of HLW from nuclear reactor fuel [4,5] with hollandite acting only as the host for radioactive cesium, barium and other large alkali ions. The general formula for Synroc hollandite was initially $[Ba_xCs_y][(Ti,Al)_{2x+y}{}^{3+}Ti_{8-2x-y}{}^{4+}]O_{16}$. Kesson and White [6] worked on this generic composition to avoid secondary phases with low chemical durability. Hollandite structure, with the general formula $A_xB_8O_{16}$ ($x \leqslant 2$), consists of double rutile chains sharing edges and corners of BO_6 octahedra to form tunnels along the *c*-axis in which A^+ or A^{2+} cations are located. The symmetry of the structure can be either tetragonal ($I4/m$) or monoclinic ($I2/m$) [7–9]. Some investigations on the optimal hollandite composition have been done by CEA within a collaboration with ANSTO and led to the formulation $Ba_1Cs_{0.28}Fe_{0.82}Al_{1.46}Ti_{5.72}O_{16}$ [10]. This formulation takes into account a possible tuning (with Fe^{III+} and Ti^{IV+}) for charge equilibrium when Cs^+ transmutation will lead to Ba^{++} during storage. Amount of cesium is limited at 5 wt% of Cs_2O in this material because of the thermogenic capacity of this element. Higher content could trigger the deterioration of the matrix. This structure permits to include cesium and barium resultant of cesium transmutation according to the reaction

$$^{13x}_{55}Cs^+ \xrightarrow{\beta^-} (^{13x}_{56}Ba^{2+})^* + e^- \xrightarrow{\gamma} {}^{13x}_{56}Ba^{2+} + \gamma$$

with ($x = 4, 5$ or 7).

Structure accommodation to cesium transmutation is possible with reduction of Ti(IV) into Ti(III) or Fe(III) into Fe(II). Our study consists in physicochemical characterization of this material and, more precisely, in its structural characterization and Cs location.

2. Experimental section

2.1. Synthesis

$Ba_1Cs_{0.28}Fe_{0.82}Al_{1.46}Ti_{5.72}O_{16}$ hollandite is prepared either by an alcoxyde route or a dry route. The former has been developed by CEA [10] using alcoxydes for titanium and aluminum, and nitrates for iron, barium and cesium as pristine materials. Alcoxydes, in proper amounts, are mixed together in pure ethanol, and poured drop by drop in the aqueous nitrate solution. After vigorous stirring, evaporation of the solvents with a rotavapor, and a drying at 100 °C, the powder precursor was prefired at 1000 °C during 2 h in alumina crucibles, then milled, pressed into pellet ($\Phi = 28$ mm) under 120 MPa and sintered at 1200 °C during 15 h. This synthesis is well adapted for preparing large quantities (beyond 100 g), but lead to the stabilization of TiO_2 rutile as impurity for low amount (few grams).

The dry route has been developed for the laboratory scale. Anatase TiO_2, $Al(NO_3)_3 \cdot 9H_2O$, $Fe(NO_3)_3 \cdot 9H_2O$, $CsNO_3$ and $BaCO_3$ were mixed in stoichiometric proportion in an agate mortar. After calcination at 1000 °C for 6 h (1 °C/min) in alumina crucibles, the hollandite was found to be pure, as determined from chemical analysis from energy-dispersive X-ray spectroscopy (EDXS) using both scanning electron microscopy (SEM) and transmission electron microscopy (TEM): both techniques, whatever the observation scale, give the expected formulation within standard uncertainties for an average formulation based on 10 different measurement points ($Ba_1Cs_{0.28}Fe_{0.82}Al_{1.46}Ti_{5.72}O_{16}$ hollandite is analyzed as $Ba_{1.1}Cs_{0.3}Fe_{0.8}Al_{1.5}Ti_{5.7}O_{16}$ with a standard uncertainty of 3%.). In addition, no extra Bragg peak was observed on the diffraction pattern. Vide infra for experiment technical details. After this calcination step, the material was then pressed into pellet ($\Phi = 13$ mm) under 120 MPa and sintered at 1200 °C during 15 h.

Samples obtained by these two routes were similar after sintering at 1200 °C from the crystallographic and morphologic points of view.

2.2. Characterization method

Different techniques have been envisaged for chemical analysis of the synthesized materials like induction-coupled plasma (ICP), flame emission spectrometry (FES), but the dissolution of the studied material presents an important problem. Therefore, only results on EDXS have been exploited.

2.2.1. EDX spectroscopy

Analyses have been done using EDXS on a JEOL 5800 SEM (scanning electron microscope). Samples were

pelletized ($\Phi = 13$ mm, under 250 MPa) in order to minimize errors related to their roughness. Oxygen percentage was not taken into account and other percentages were normalized assuming $Fe + Al + Ti = 8$ in a $Ba_xTi_8O_{16}$-like formulation. However, this technique neither takes into account the electroneutrality nor a possible non-stoichiometry.

2.2.2. Mössbauer spectroscopy

For the ^{57}Fe Mössbauer study, the powdered samples were put into sample holders, which were then glued. Mössbauer measurements were performed using a conventional constant acceleration spectrometer WissEl Canberra provided with a ^{57}Co(Rh) source and using an Oxford Instruments cryostat for measurements down to 78 K. The hyperfine parameters were refined using least-square fitting procedure. Isomer shift values refer to α-Fe at 300 K.

2.2.3. X-ray absorption near edge structure (XANES) spectroscopy

XANES experiments have been done at the Laboratoire pour l'Utilisation du Rayonnement Electromagnétique (LURE). The references used as indicator of Ti^{II+}, Ti^{III+} and Ti^{IV+} were, respectively, TiO, Ti_2O_3 and rutile TiO_2. All the spectra (references and sample) were recorded at the Ti-*K* absorption edge (4.966 keV).

2.2.4. Laboratory X-ray diffraction (XRD)

XRD was performed using an INEL or a Siemens D5000 diffractometer at a controlled temperature of 293 K. The INEL one is in a Debye–Scherrer geometry using the CuK–L_3 copper radiation ($\lambda = 1.540598$ Å), thanks to a bent quartz monochromator. The sample filled a 0.2 mm in diameter Lindemann capillary. This technique allows the use of tiny amount of powder and prevents greatly from preferred orientation. Siemens D5000 diffractometer is set up in a Bragg–Brentano geometry with a copper anode (CuK–L_2,L_3, $\lambda = 1.540598$ and 1.544390 Å). The powder was placed on a plate with circular recess and scraped flush with the surface using a ground glass slide to minimize any preferred grain orientation. The plate was then positioned so that the sample surface was perfectly flat and tangential to the goniometer focusing circle. Patterns were collected from 15° to 115° in 2θ. Rietveld refinements were performed with JANA 2000 [11] and Fullprof.2000 program [12] for phase quantification. This technique has some limitation: barium and cesium cannot be distinguished from X-ray diffraction with copper radiation. This is the reason why the electronic density in the tunnel was assumed to correspond to only one species. For titanium, iron and aluminum occupying the same site, the impossibility to refine the electronic density distribution on more than two atoms occupying the same site imposes to refine only two of them (Ti and Al) or to fix them at the expected values. Therefore, a non-stoichiometry on the *B* site cannot be observed by this technique. Also, XRD is not quite sensitive to light elements like oxygen. Thus, its occupation rates have not been refined.

2.2.5. Resonant XRD

XRD cannot differentiate two elements close in the periodic table using the acquisition usual conditions. A scattering power contrast can be obtained near the absorption edge of one of these elements, permitting the distinction of those two elements. Therefore, some specimens were studied by synchrotron radiation at The European Synchrotron Radiation Facility (ESRF) in Grenoble (France) on the Swiss Norwegian Beam line (SNBL) near the Ba-*K* and Cs-*K* absorption edges to obtain a barium and cesium contrast and far from the edges to obtain general information. The samples were primarily sieved down to 20 μm and then placed in a 0.5 mm in diameter Lindemann capillary. The Rietica program [13] was used for multipattern Rietveld refinements, a simultaneous refinement of several patterns corresponding to the same structure. Correction of resonant diffusion coefficients f' and f'' tabulated in the literature [14] are not accurate enough to give correct information close to absorption edges where their variation is huge. Those factors can be calculated with the CHOOCH program [15] with X-ray absorption measurements at barium and cesium edges. These values were found to be $f' = -7.76$ and $f'' = 1.17$ and $f' = -8.05$ and $f'' = 1.32$ for Ba and Cs edges, respectively.

The Rietveld refinement strategy used for all the data was the same whatever the program used: the background was refined using a Chebychev polynomial (excepted for Fullprof where a six-term polynomial was used), the line profile was the modified Thompson–Cox–Hastings pseudo-Voigt function [16], no preferred orientation correction was used since we succeed to minimize this effect during the sample preparation (any attempt to refine this parameter led to a value close to zero within the standard uncertainty), no asymmetry corrections were necessary as no important Bragg peaks are found below 28° 2θ. For all the patterns collected in the Bragg–Brentano geometry, a sample height correction parameter was refined. For all the refinements, excepted in Table 6 (see below), the correlation between atomic displacement parameter and site occupancy, that could be important, was checked through the correlation matrix. It was also checked that, for a given atom, the couple of values for these two parameters did not change within standard uncertainty from cycle to cycle. In addition, the site occupation fraction, especially for Ba And Cs, was compared to the expected value deduced from the chemical analysis and always found to be in very good agreement within standard uncertainty.

2.2.6. Ionic conductivity

Ionic conductivity was measured by complex impedance on an inductometer Solartron 1260 in the 10^2 to 2×10^6 Hz range, from 320 to 800 °C on sintered pellets gilded on the two faces.

2.2.7. TEM

Electron diffraction (ED) as EDXS analysis was carried out on a Philips-CM30 microscope at 300 kV. Polycrystalline ceramic fragments were ground in ethanol and dispersed onto holey carbonaceous support films of polymers. EDXS was done with the Link ISIS software 3.32, 1992–1997, Oxford Instruments plc.

3. Results and discussion

3.1. After sintering at 1200 °C

The two different synthesis routes give same results after sintering at 1200 °C. Chemical analysis with EDXS on SEM gives the composition "$Ba_{1.3}Cs_{0.3}Fe_{0.8}Al_{1.3}Ti_{5.9}O_{16}$" (average on 14 analyses), in good agreement with the expected one: $Ba_1Cs_{0.28}Fe_{0.82}Al_{1.46}Ti_{5.72}O_{16}$.

After sintering, the iron oxidation state has been studied by Mössbauer spectroscopy to characterize perfectly the final material. At room temperature, the observed spectrum (Fig. 1) is a centered doublet at 0.37 mm/s, which corresponds to the characteristic Fe^{III+} high spin isomer shift (0.38 mm/s for Fe_2O_3-α) with a quadrupolar splitting at 0.26 mm/s. The half-width at half-maximum (HWHM) is a little large (0.18 mm/s against 0.11 mm/s for the sodium nitroprusside, $Na_2Fe(CN)_5NO$, used for calibration) and the doublet is asymmetrical.

To explain this asymmetry, a small contribution of Fe^{II+} has been envisaged. However, this hypothesis implicates another peak around 2.2 mm/s not present on the spectrum and it does not lead to a perfect modeling of the asymmetry. A new hypothesis has been tested: the presence of two or more Fe^{III+} sites. This hypothesis permits to explain the peak shape but is not realistic because one of the sites has a HWHM >0.20 mm/s and the refinement can give a multitude of solutions. The last hypothesis envisaged is a thermal anisotropy of vibration of the Mössbauer atom (Goldanskii–Kariagin effect) [17].

Thus, a new data collection has been done at 78 K to lower thermal vibration. The obtained spectrum is symmetrical (Fig. 1), confirming the hypothesis that the asymmetry, at room temperature, is caused by the Goldanskii–Kariagin effect.

The large width of the doublet can be explained by the presence in the tunnel of Ba, Cs or vacancy and the alternation of Fe with Ti and Al in the cationic skeleton. It can be modeled with only one site of Fe^{III+} but in reality it corresponds to a multitude of sites different because of their second neighbors. Therefore, this sample is composed only of Fe^{+III} ($\pm 3\%$) in good agreement with the theoretical value.

XANES measurements have also been done on this sample. The edge observed on the spectra of our sample corresponds to that of rutile. These results confirm that this sample is only composed of Ti^{+IV} ($\pm 5\%$), as expected.

The hollandite $Ba_1Cs_{0.28}Fe_{0.82}Al_{1.46}Ti_{5.72}O_{16}$ has been studied by laboratory XRD on the INEL diffractometer. Its symmetry after sintering is tetragonal (space group $I4/m$) as expected ($a = 10.0458(1)$ Å, $c = 2.94185(5)$ Å). Indeed, according to the literature [8], when hollandite

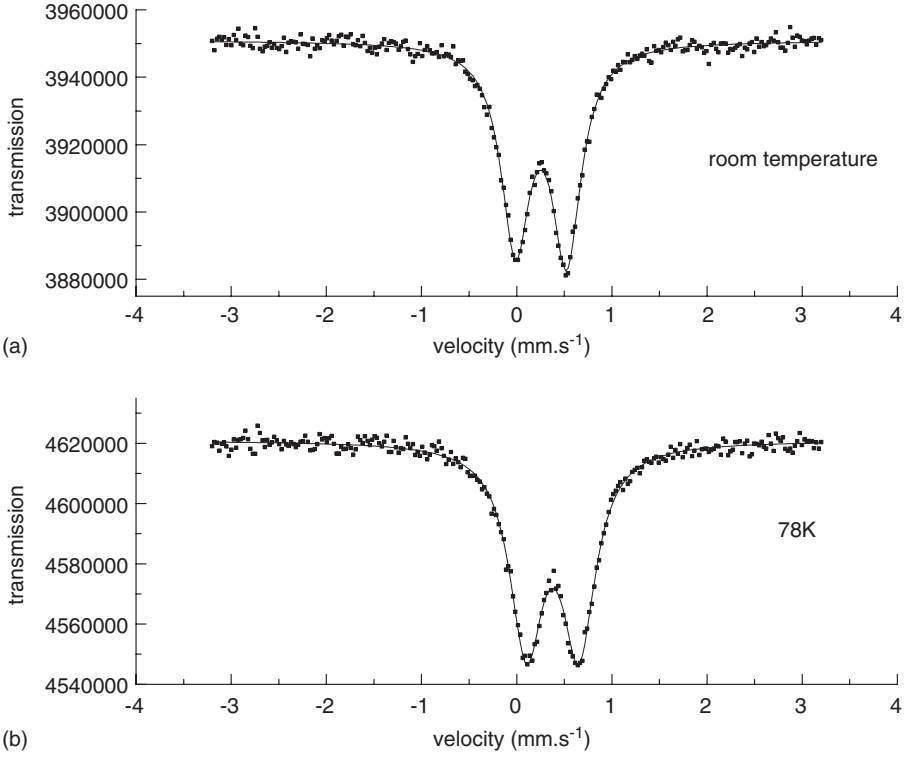

Fig. 1. Mössbauer spectra of sintered hollandite: (a) at room temperature and (b) at 78 K.

contains cesium, its symmetry is tetragonal because of the biggest size of cesium compared to barium ($r_{Cs} = 1.74$ Å and $r_{Ba} = 1.42$ Å). Rietveld refinement results are gathered in Table 1 and Fig. 2. For titanium, iron and aluminum occupying the same site, only two of those (Ti and Al) have been introduced in this refinement. These two elements introduced in the refinement were chosen to try to refine aluminum occupation rate in one hand and iron–titanium in the other hand, without any success. With laboratory XRD, the tunnel site occupancy (Ba and Cs) is refined to 1.2 per 16 oxygen atoms, in good agreement with EDXS-SEM and with the theoretical value.

To localize exactly cesium in this structure, data collections near Ba and Cs edges have been done. A first experiment far from edges permits to obtain general information on two sites for Ba and Cs, then the recording near Ba and Cs edges permits to enhance barium and cesium density, respectively, on those sites. Rietveld refinement was done using simultaneously the following three patterns. In such a kind of experiment, the absolute value of the wavelengths is not accurate enough. Thus, the unit cell parameters values were fixed to those previously determined using a classical CuK–L_3 anode available in our lab, as reported in Table 1 ($a = 10.0458(1)$ Å, $c = 2.94185(5)$ Å), the wavelengths being refined. From these accurate wavelength values, a linear absorption coefficient was calculated to take into account absorption corrections ($r = 0.5$ mm, powder compactness = 35%), in a Debye–Scherrer geometry.

Results of this refinement are gathered in Table 2 and Fig. 3, that show two distinct sites for barium and cesium. Barium occupancy rate was refined, but it remains close to 0.25 and thus it was decided to fix it to 1/4. For Ti, Fe and Al, site occupancies were fixed at the expected values (to assume a $Ba_1Cs_{0.28}Fe_{0.82}Al_{1.46}Ti_{5.72}O_{16}$ composition) because of the impossibility to refine the electronic density distribution on more than two atoms occupying the same site. Wavelengths were refined preliminary to values indicated in Table 2. The composition extrapolated from these results is "$Ba_1Cs_{0.22}Fe_{0.82}Al_{1.46}Ti_{5.72}O_{16}$" enhancing the cesium loss expected at the end of the synthesis after thermal treatment (calcination at 1000 °C and sintering at 1200 °C). One can note in Fig. 3 the presence of two broad unexplained peaks around 5° 2θ. These peaks are due to the presence of an incommensurate modulation of the hollandite phase, with a wave vector distribution [18].

Barium and cesium in the sintered hollandite do not have the same position in the tunnel as reported in Table 2. Cesium and barium displacement parameters are the same within standard deviation, the error is more important on the cesium one, because of the lower occupation rate of this element. Representation of the unit cell along tunnel axis (c-axis) in Fig. 4 and the bond length presented in Table 3 illustrate that barium is more centered than cesium in tunnel axis of the hollandite $Ba_1Cs_{0.28}Fe_{0.82}Al_{1.46}Ti_{5.72}O_{16}$. This observation does not corroborate with Cheary's hypothesis [19]: Cheary presents barium with an ionic

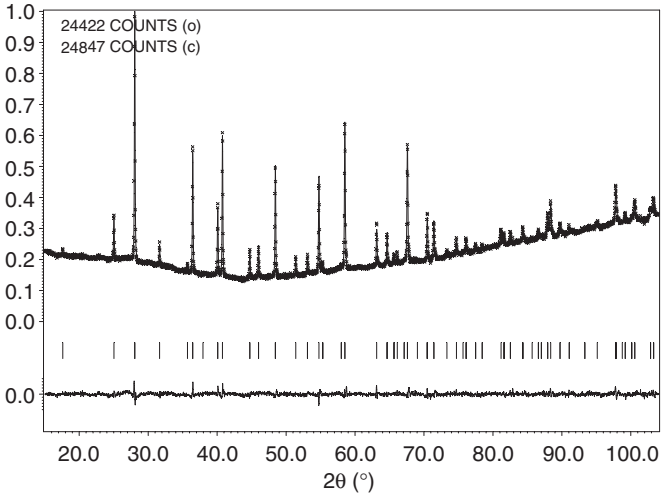

Fig. 2. Refinement (JANA) of the sintered $Ba_1Cs_{0.28}Fe_{0.82}Al_{1.46}Ti_{5.72}O_{16}$ hollandite structure (laboratory XRD pattern collected on an INEL diffractometer ($\lambda_1 = 1.540598$ Å).

Table 1
Refinement (JANA) of the sintered $Ba_1Cs_{0.28}Fe_{0.82}Al_{1.46}Ti_{5.72}O_{16}$ hollandite structure (laboratory XRD pattern collected on an INEL diffractometer ($\lambda_1 = 1.540598$ Å)

Space group	Volume (Å^3)	Cell parameters (Å)	
		a	c
$I4/m$	296.887 (6)	10.0458 (1)	2.94185 (4)

Atoms	Site	x	y	z	U	Occupation
Ba/Cs	4e	0	0	0.602(4)	0.030(4)	0.3(1)
Ti	8h	0.3520(3)	0.1673(3)	0	0.0022(7)	0.680(9)
Al	8h	0.352	0.1673	0	0.0022	0.320(9)
O1	8h	0.1537(7)	0.2045(6)	0	0.0132(15)	1
O2	8h	0.5409(6)	0.1654(9)	0	0.0132	1

$R_p = 1.63$ $R_{wp} = 2.19$ $R_{exp} = 1.34$ $R_{BRAGG} = 3.02$

Table 2
Refinement (RIETICA) of the sintered $Ba_1Cs_{0.28}Fe_{0.82}Al_{1.46}Ti_{5.72}O_{16}$ hollandite structure (synchrotron patterns collected far from edges, near Ba edge and near Cs edge)

Space group	Volume (Å^3)	Cell parameters (Å)	
		a	*c*
*I*4/*m*	297.022	10.0458	2.94185

Atoms	Site	*x*	*y*	*z*	*U*	Occupation
Ba	4*e*	0	0	0.407(1)	0.0191(6)	0.25
Cs	4*e*	0	0	0.291(4)	0.009(2)	0.056(3)
Ti	8*h*	0.3510(1)	0.1671(1)	0	0.00722(13)	0.715
Al	8*h*	0.351	0.1671	0	0.00722	0.1825
Fe	8*h*	0.351	0.1671	0	0.00722	0.1025
O1	8*h*	0.1568(2)	0.2034(2)	0	0.0167(19)	1
O2	8*h*	0.5408(2)	0.1669(2)	0	0.0167	1

Far from edges	$\lambda = 0.50005$ Å	$R_p = 6.07$	$R_{wp} = 7.84$	$R_{exp} = 5.16$	$R_{BRAGG} = 2.19$
Ba edge	$\lambda = 0.331363$ Å	$R_p = 2.71$	$R_{wp} = 3.65$	$R_{exp} = 2.70$	$R_{BRAGG} = 1.99$
Cs edge	$\lambda = 0.344496$ Å	$R_p = 3.46$	$R_{wp} = 4.66$	$R_{exp} = 2.68$	$R_{BRAGG} = 1.99$

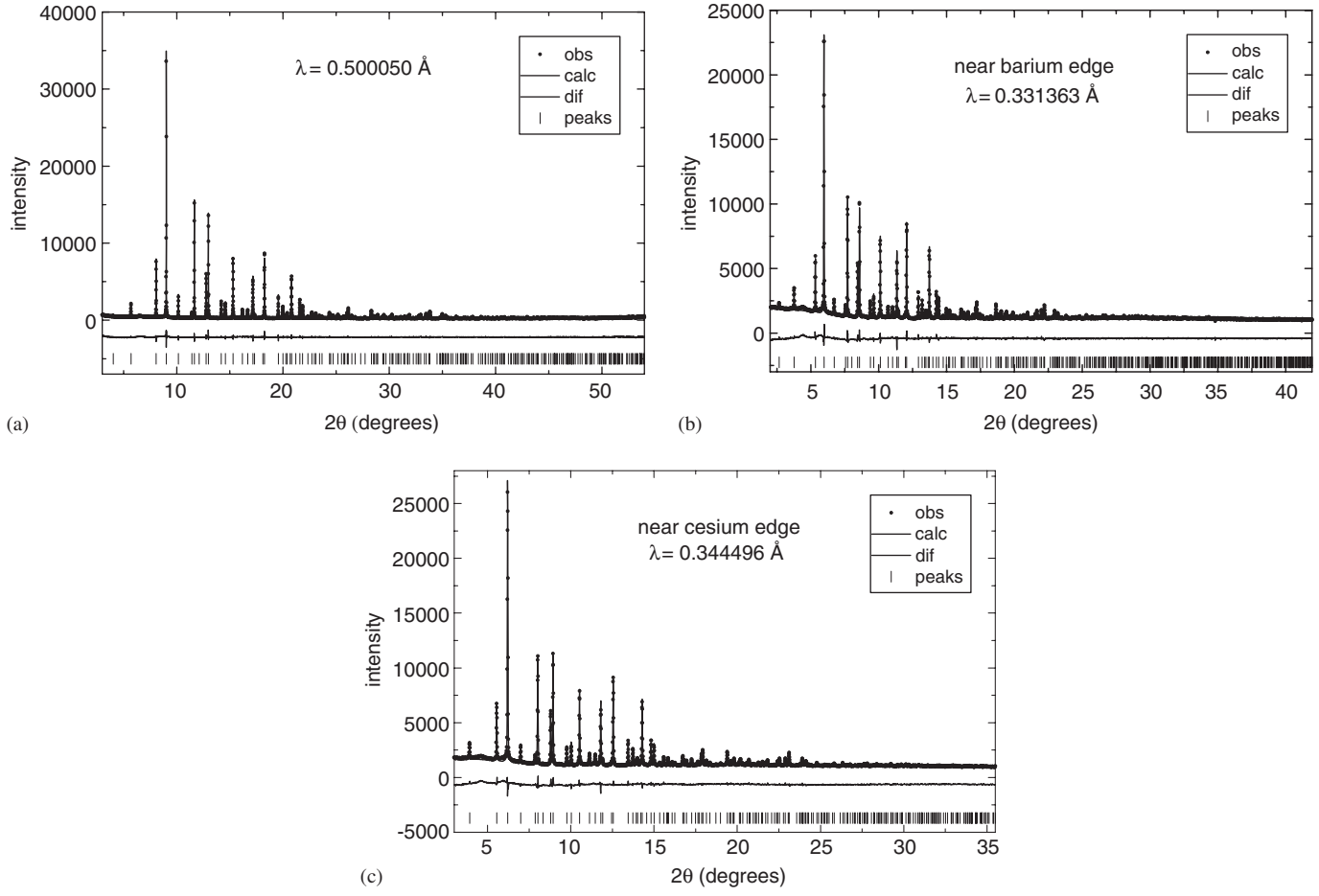

Fig. 3. Refinement (RIETICA) of the sintered $Ba_1Cs_{0.28}Fe_{0.82}Al_{1.46}Ti_{5.72}O_{16}$ hollandite structure (synchrotron patterns collected far from edges, near Ba edge and near Cs edge).

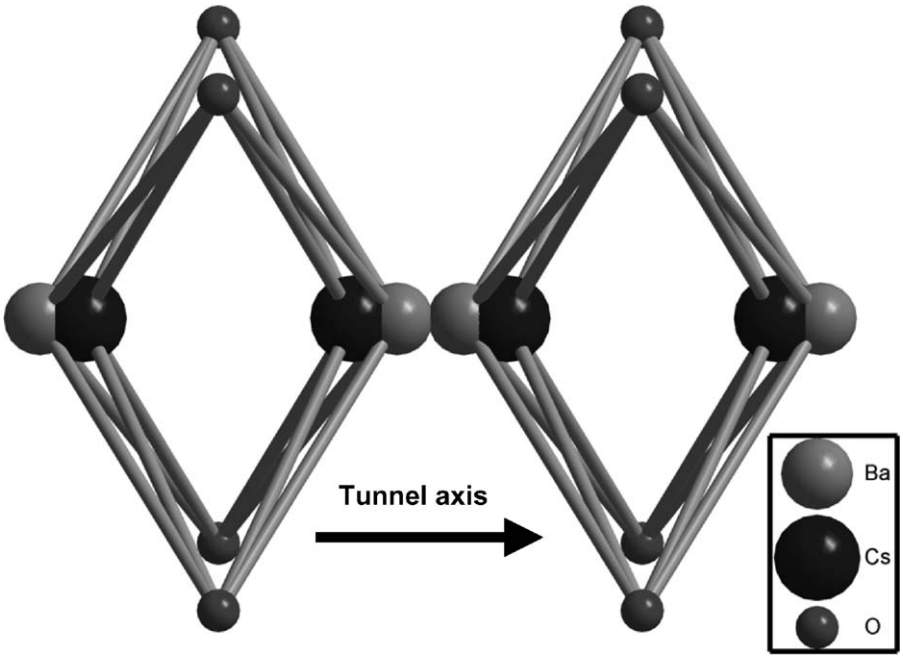

Fig. 4. Sintered hollandite structure representation perpendicular to the tunnel axis.

Table 3
Listing of the distances between barium or cesium and oxygen in the sintered $Ba_1Cs_{0.28}Fe_{0.82}Al_{1.46}Ti_{5.72}O_{16}$ hollandite (RIETICA program)

Distances (Å)	Ba	Cs
O1	2.846(2)	2.712(2)
O1	3.115(2)	3.333(2)
O2	3.379(2)	3.427(2)

radius smaller than the tunnel cavities, occupying off-centered locations, and cesium ion larger than those cavities accommodated a central position with a localized deformation of oxygen atoms around the tunnel site. Those hypotheses are based on the comparison of Cs-free hollandite and hollandite containing Ba and Cs, but no real distinction between those two elements has been done.

At this stage, let us notice that Hollandite material is also studied as positive material for rechargeable batteries [20]. This application seems to be opposite to radioactive storage were cation mobility in the tunnels has to be as small as possible. Ionic conductivity is then an important property to study. It has been measured for the sintered hollandite $Ba_1Cs_{0.28}Fe_{0.82}Al_{1.46}Ti_{5.72}O_{16}$ by complex impedance (Fig. 5). Under 320 °C, conductivity was under the detection limit of the equipment, so less than 10^{-9} S/cm. The activation energy was estimated at 1.37 eV. In the same condition, for a $K_{1.6}Mg_{0.77}Ti_{7.23}O_{16}$ hollandite, the activation energy was lower: 0.23 eV [21]. Results obtained on hollandite $Ba_1Cs_{0.28}Fe_{0.82}Al_{1.46}Ti_{5.72}O_{16}$ prove that this material is a weak ionic conductor, in good agreement with leaching tests [22] indicating a very low Cs release. In fact, this low mobility of cesium can be due to the presence of

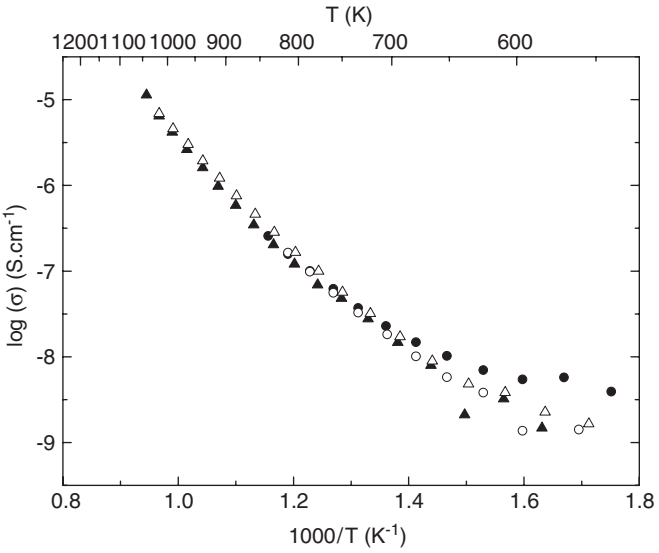

Fig. 5. Ionic conductivity measurement on sintered hollandite Black: temperature increase; open: temperature decrease; ●: first; ▲: second.

barium less mobile because of its higher charge, and also to the bottleneck due to the O1 anions.

To understand Cs behavior in the tunnels, it was decided to look at the formation of the *I*4/*m*-type symmetry, therefore, to study the material obtained at the end of the first reaction step (i.e., the calcination step at 1000 °C carried out just prior to sintering at 1200 °C).

3.2. After calcinations at 1000 °C

After calcination, the two synthesis routes are not equivalent.

Firstly, the interest related to samples obtained by the dry route. By EDXS with SEM, the composition "$Ba_{1.2}Cs_{0.3}Fe_{1.1}Al_{1.4}Ti_{5.5}O_{16}$" (average on four analyses) is not to far from the theoretical one $Ba_1Cs_{0.28}Fe_{0.82}Al_{1.46}Ti_{5.72}O_{16}$.

This route gives rise to a tetragonal hollandite, observed by laboratory XRD on the D5000 diffractometer, from the calcination. Results are reported in Table 4. The tunnel occupancy is refined at 1.26, in good agreement with the EDXS and the theory. Atomic position and occupation are similar to the sintered hollandite, the only difference comes from the cell parameters: cell parameters before sintering (i.e., after calcinations, $a = 10.0642(7)$ Å, $c = 2.94725(17)$ Å) are slightly larger than after sintering ($a = 10.0458(1)$ Å; $c = 2.94185(5)$ Å) (Scheme 2) while applying the Bérar and Lelann's factor [23], permitting to obtain more realistic errors than the underestimated ones obtained by Rietveld refinement. This difference has been seen in the three samples studied in the same conditions. This result indicates a slight composition difference (Fe/Al/Ti and O occupancy not refined) between samples before and after sintering.

Secondly, the prefired samples synthesized by alcoxyde route have been studied and give very different results.

The pattern obtained by laboratory X-ray diffraction on the Inel diffractometer cannot be explained by a pure

Table 4
Refinement (JANA2000) of the prefired $Ba_1Cs_{0.28}Fe_{0.82}Al_{1.46}Ti_{5.72}O_{16}$ hollandite structure obtained by dry route ($\lambda_1 = 1.540598$ Å, $\lambda_2 = 1.54433$ Å)

Space group	Volume (Å^3)	Cell parameters (Å)	
		a	*c*
*I*4/*m*	298.52(3)	10.0642(7)	2.94725(17)

Atoms	Site	*x*	*y*	*z*	*U*	Occupation
Ba/Cs	4*e*	0	0	0.3703(15)	0.012(3)	0.316(4)
Ti	8*h*	0.3521(5)	0.1671(5)	0	0.0054(14)	0.715
Al	8*h*	0.3521	0.1671	0	0.0054	0.1825
Fe	8*h*	0.3521	0.1671	0	0.0054	0.1025
O1	8*h*	0.1549(10)	0.2073(9)	0	0.0127(16)	1
O2	8*h*	0.5438(9)	0.1677(11)	0	0.0127	1

$R_p = 2.41$ $R_{wp} = 3.07$ $R_{exp} = 2.70$ $R_{BRAGG} = 2.63$

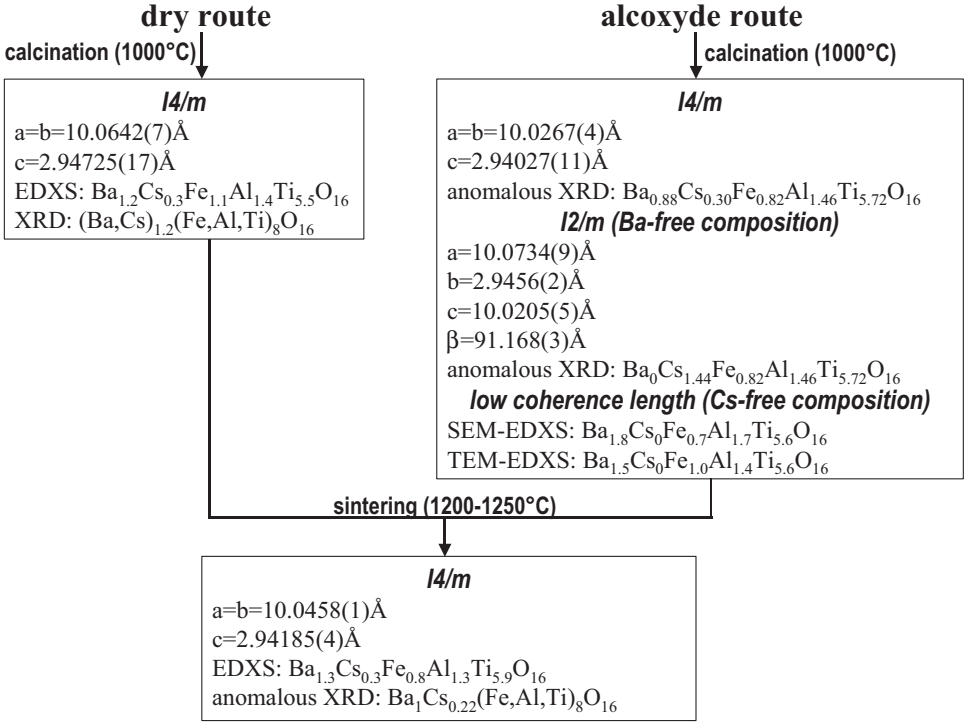

Scheme 2. Recapitulation of the synthesis results.

tetragonal hollandite ($I4/m$). A monoclinic hollandite ($I2/m$) has been tested with Rietveld refinement, but peaks profile and intensities were not well explained. The only combination explaining totally the X-ray pattern is a biphased tetragonal + monoclinic hollandite (Table 5 and Fig. 6). Shoulder on the left side of diffraction peaks in Fig. 7 corresponds to the monoclinic hollandite phase. The tetragonal hollandite seems to correspond to the sintered hollandite with the same positions and occupation rate for the different atoms, but cell parameters are different (a and c are smaller after calcination ($a = 10.0261(6)$ Å; $c = 2.9401(2)$ Å) than after sintering ($a = 10.0458(1)$ Å; $c = 2.94185(5)$ Å)). This might be explained by a different composition of the framework (Ti, Al, Fe not refined) due to the presence of other phases in the samples giving a different stoichiometry than expected.

To distinguish Cs and Ba in these two phases ($I4/m$ and $I2/m$), data collections near Ba and Cs edges have been done as for the pure $I4/m$ phase obtained after sintering at 1200 °C. Those experiments have been done to quantify and localize barium and cesium in the two phases. The multipattern refinement was carried out as described in the experimental section. In contrast with the sintered case, cell parameters and the wavelength far from edges, different than the one used for sintered hollandite, were refined and

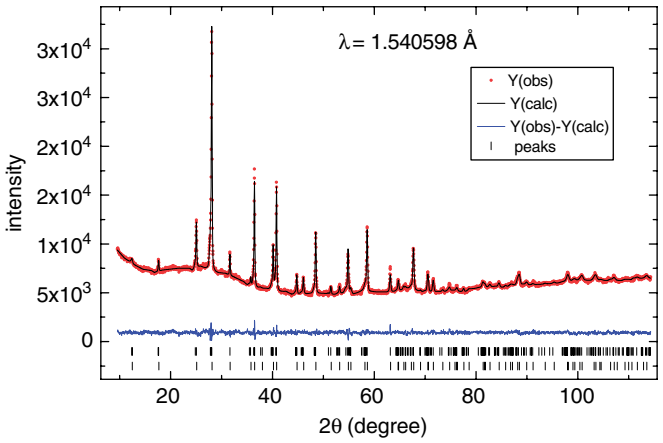

Fig. 6. Refinement (FullProf) of the prefired $Ba_1Cs_{0.28}Fe_{0.82}Al_{1.46}Ti_{5.72}O_{16}$ hollandite with the coexistence of $I4/m$ and $I2/m$ phases (XRD pattern collected on an INEL diffractometer, $\lambda = 1.540598$ Å).

Table 5
Refinement (FullProf) of the prefired $Ba_1Cs_{0.28}Fe_{0.82}Al_{1.46}Ti_{5.72}O_{16}$ hollandite with the coexistence of $I4/m$ and $I2/m$ phases (XRD pattern collected on an INEL diffractometer, $\lambda = 1.540598$ Å)

Phase 1	Space group	Cell parameters (Å)	
		a	c
Tetragonal	$I4/m$	10.0261(6)	2.9401(2)

Atoms	Site	x	y	z	U	Occupation
Ba/Cs	4e	0	0	0.567(8)	0.042(6)	0.292(7)
Ti	8h	0.3511(8)	0.1660(9)	0	0.003(2)	0.76(6)
Al	8h	0.3511	0.1660	0	0.003	0.24(6)
O1	8h	0.154(2)	0.201(2)	0	0.010(6)	1
O2	8h	0.538(2)	0.167(2)	0	0.010	1
		$R_{bragg} = 5.36$			$wt\% = 57(7)\%$	

Phase 2	Space group	Cell parameters (Å)			
		a	b	c	β
Monoclinic	$I2/m$	10.109(7)	2.943(1)	10.053(8)	90.45(7)

Atomes	Site	x	y	z	U	Occupation
Ba/Cs	4g	0	0.66(2)	0	0.05(2)	0.3(2)
Ti1	4i	0.154(6)	0	0.362(5)	0.046(10)	0.7(2)
Al1	4i	0.154	0	0.362	0.046	0.3(2)
Ti2	4i	0.649(4)	0	0.18(6)	0.046(10)	0.8(3)
Al2	4i	0.649	0	0.18	0.046	0.2(3)
O1	4i	0.180(8)	0	0.15(1)	0.01(2)	1
O2	4i	0.87(1)	0	0.215(8)	0.01(2)	1
O3	4i	0.166(9)	0	0.53(1)	0.01(2)	1
O4	4i	0.46(1)	0	0.13(1)	0.01(2)	1
		$R_{Bragg} = 10.1$			wt% = 43(9)%	
$R_p = 1.51$		$R_{wp} = 1.97$		$R_{exp} = 1.25$		$\chi^2 = 2.45$

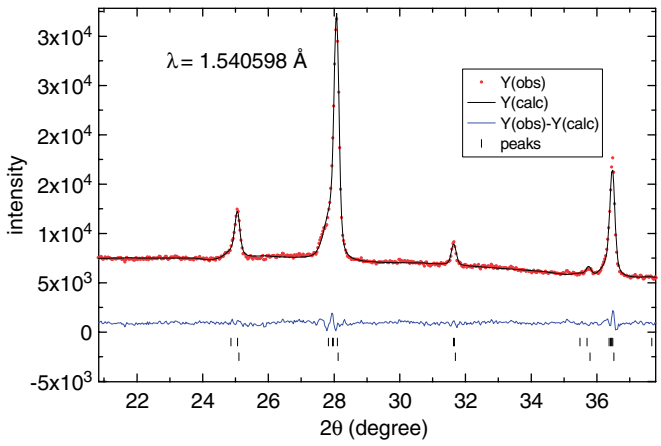

Fig. 7. Enlarged view of the X-ray diffraction pattern of prefired samples obtained by alcoxyde route with the coexistence of *I*4/*m* and *I*2/*m* hollandite (FullProf).

wavelengths near Ba and Cs edges were fixed at the values obtained on the sintered hollandite in Table 2. Contrary to Table 2 where the *I*4/*m* phase is alone, the coexistence of *I*4/*m* and *I*2/*m* phases (vide infra and Table 6) leads to a more complicated situation implying to fix the Cs and Ba atomic displacement parameters to the values found in Table 2. This allowed us to extract accurate site occupation fractions for both Ba and Cs and, thus, to obtain an important chemical information on the two coexisting phases. The resolution of the patterns obtained on synchrotron is better than those obtained in the laboratory. Then, with those data collections, the presence of a tetragonal and a monoclinic hollandite in this sample is confirmed and more precisely refined. Results are summarized in Table 6, giving resulting patterns as in Fig. 8. In this figure, the presence of bumps has been observed and will be discussed in a future paper. Percentages obtained in this

Table 6
Refinement (RIETICA) of the prefired $Ba_1Cs_{0.28}Fe_{0.82}Al_{1.46}Ti_{5.72}O_{16}$ hollandite with the coexistence of of *I*4/*m* and *I*2/*m* phases (synchrotron XRD patterns)

Phase 1	Space group	Cell parameters (Å)	
		a	*c*
Tetragonal	*I*4/*m*	10.0267(4)	2.94027(11)

Atoms	Site	*x*	*y*	*z*	*U*	Occupation
Ba	4*e*	0	0	0.422(4)	0.0190	0.220(12)
Cs	4*e*	0	0	0.322(7)	0.0094	0.076(12)
Ti	8*h*	0.35132(11)	0.16737(11)	0	0.0062	0.715
Al	8*h*	0.35132	0.16737	0	0.0062	0.1825
Fe	8*h*	0.35132	0.16737	0	0.0062	0.1025
O1	8*h*	0.1552(3)	0.2022(3)	0	0.0063	1
O2	8*h*	0.5417(3)	0.1679(3)	0	0.0063	1

wt% = 74.8(4)%

Phase 2	Space group	Cell parameters (Å)			
		a	*b*	*c*	*β*
Monoclinic	*I*2/*m*	10.0734(9)	2.9456(2)	10.0205(5)	91.168(3)

Atoms	Site	*x*	*y*	*z*	*U*	Occupation
Ba	4*g*	0	0.40(10)	0	0.0190	−0.004(40)
Cs	4*g*	0	0.658(5)	0	0.0089	0.36(4)
Ti1	4*i*	0.1652(8)	0	0.3428(10)	0.0076	0.715
Al1	4*i*	0.1652	0	0.3428	0.0076	0.1826
Fe1	4*i*	0.1652	0	0.3428	0.0076	0.1024
Ti2	4*i*	0.6563(8)	0	0.1640(12)	0.0076	0.715
Al2	4*i*	0.6563	0	0.1640	0.0076	0.1826
Fe1	4*i*	0.6563	0	0.1640	0.0076	0.1024
O1	4*i*	0.2210(19)	0	0.183(3)	0.0063	1
O2	4*i*	0.8244(17)	0	0.232(3)	0.0063	1
O3	4*i*	0.1749(16)	0	0.531(3)	0.0063	1
O4	4*i*	0.452(2)	0	0.174(3)	0.0063	1

wt% = 25.2(3)

Far from edges	$\lambda = 0.519740(12)$ Å	$R_p = 5.42$	$R_{wp} = 7.34$	$R_{BRAGG} = 4.42$
Near Ba edges	$\lambda = 0.331363$ Å	$R_p = 3.09$	$R_{wp} = 4.52$	$R_{BRAGG} = 2.92$
Near Cs edges	$\lambda = 0.344496$ Å	$R_p = 2.82$	$R_{wp} = 3.91$	$R_{BRAGG} = 2.43$

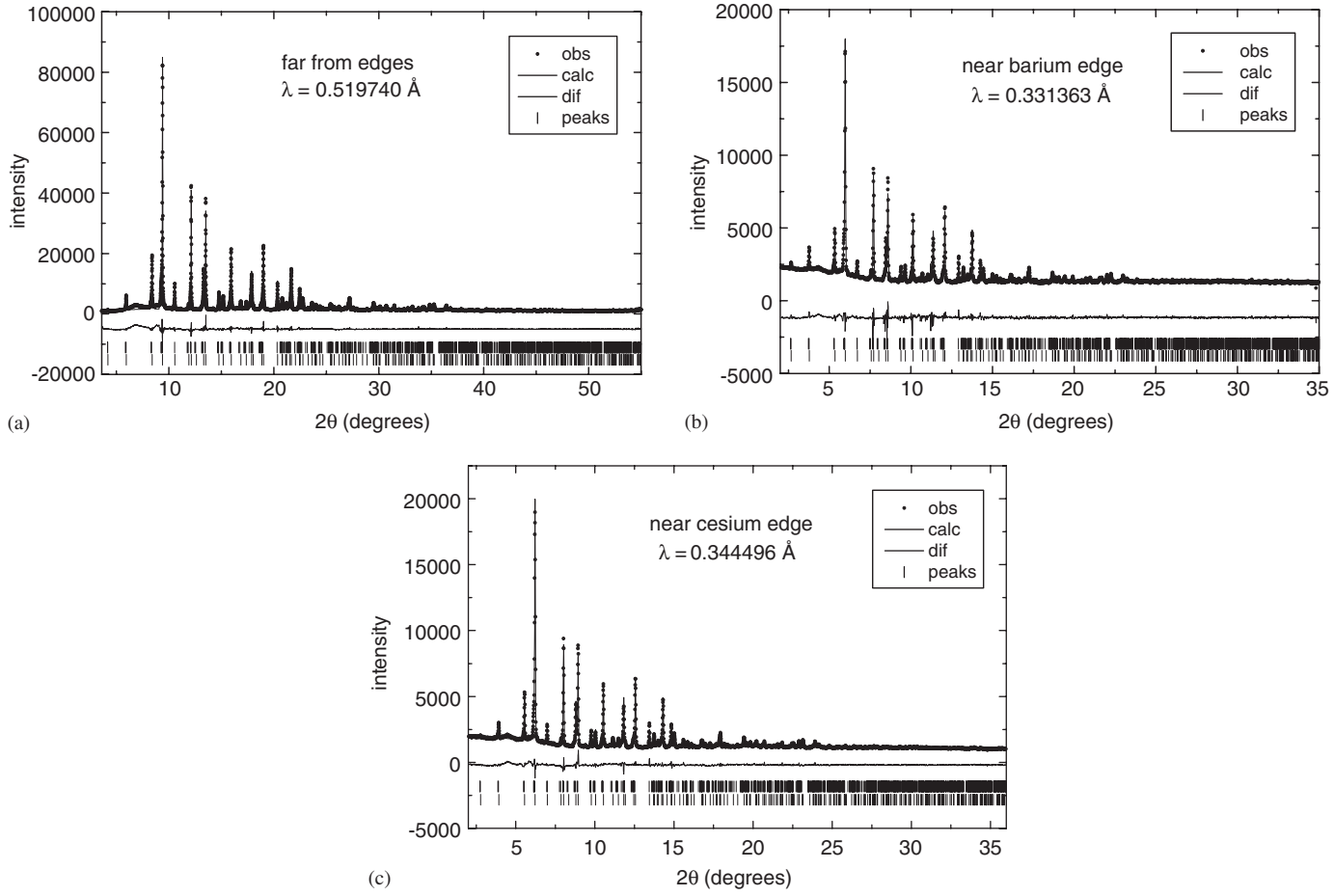

Fig. 8. Refinement (RIETICA) of the prefired $Ba_1Cs_{0.28}Fe_{0.82}Al_{1.46}Ti_{5.72}O_{16}$ hollandite with the coexistence of $I4/m$ and $I2/m$ phases (synchrotron XRD patterns).

refinement take into account the hypothesis that Fe, Al and Ti occupations are fixed at the targeted values in the two phases (monoclinic and tetragonal). They are in good agreement with those obtained by laboratory XRD except a difference in the monoclinic cell parameters. It can be explained by the strong overlapping of the two phases, leading to larger uncertainty with laboratory XRD because of lower instrumental resolution. The tetragonal phase, accounting for 74.8(4) wt% of crystallized phases, is not far from the hollandite obtained after sintering: Ba and Cs have the same position and occupation than after sintering, only the cell parameters are different. Composition obtained from the Rietveld refinement (where Fe, Al and Ti site occupancy is fixed for the reason mentioned above) "$Ba_{0.88}Cs_{0.30}Fe_{0.82}Al_{1.46}Ti_{5.72}O_{16}$" is close to what is expected ($Ba_1Cs_{0.28}Fe_{0.82}Al_{1.46}Ti_{5.72}O_{16}$). The monoclinic phase, corresponding to 25.2(3) wt% of crystallized phases, is a barium-free composition ("$Ba_0Cs_{1.44}Fe_{0.82}Al_{1.46}Ti_{5.72}O_{16}$"). This observation is really original considering literature [19,24] where no hollandite with cesium has been reported to be monoclinic. This monoclinic distortion permits to increase the tunnel size and exclude short (Cs–O_1) bond (= 2.712(2) Å < 1.74 Å(r_{Cs}) + 1.40 Å(r_O) [25]) presented in Table 3 that was found in the tetragonal symmetry (Fig. 9). The tunnel frame is reorganized to accommodate Cs (Table 7). In the monoclinic hollandite, cesium is more centered in the cubic oxygen site than in tetragonal hollandite as shown in Fig. 10, but less than barium. Therefore, Cheary's observations on the central position for cesium [19] are not applicable to the compositions under study: cesium is off-centered in the $Ba_xCs_y(Fe,Al,Ti)_8O_{16}$ hollandite.

Considering the theoretical composition $Ba_1Cs_{0.28}Fe_{0.82}Al_{1.46}Ti_{5.72}O_{16}$ and the two phases obtained by XRD: $Ba_{0.88}Cs_{0.30}Fe_{0.82}Al_{1.46}Ti_{5.72}O_{16}$ (the tetragonal one) and $Ba_0Cs_{1.44}Fe_{0.82}Al_{1.46}Ti_{5.72}O_{16}$ (the monoclinic one) and their percentage (respectively around 75–25 wt%), a barium lack is obvious. An amorphous phase containing mainly or only barium has to be considered.

By SEM-EDXS, those three phases (tetragonal and monoclinic hollandite and the amorphous suspected phase) have been found. Only two different phases are observed: a first one "$Ba_{1.3}Cs_{0.3}Fe_{0.8}Al_{1.5}Ti_{5.7}O_{16}$" very similar to the theoretical composition $Ba_1Cs_{0.28}Fe_{0.82}Al_{1.46}Ti_{5.72}O_{16}$, and another Cs-free composition "$Ba_{1.8}Cs_0Fe_{0.7}Al_{1.7}Ti_{5.6}O_{16}$" (average on 21 analyses). The first phase should be a mixture of the tetragonal hollandite, the expected

one, and the monoclinic one with Ba-free composition. The second phase may correspond to the amorphous phase evoked before, with a Cs-free composition. Chemical analysis of this poly-phased material has been very difficult because of the intimate mixture of those three phases.

To verify those assumptions, EDXS coupled with ED was performed. Two phases were observed: a first one, presented as clusters, contains Ba and Cs "$Ba_{1.4}Cs_{0.3}Fe_{1.0}Al_{1.4}Ti_{5.6}O_{16}$" corresponding to a mixture of tetragonal and monoclinic hollandite observed by XRD, the second one has the composition "$Ba_{1.5}Cs_0Fe_{1.0}Al_{1.4}Ti_{5.6}O_{16}$" which corresponds to the amorphous phase inferred from XRD. Contrary to expectation, this phase was found to be crystallized by ED because of a 100 times lower wavelength (0.0225 and 1.540598 Å for ED and XRD, respectively). Hence, particles with smaller coherence length can be seen as crystallized in ED while their signature is absent in an XRD pattern. Unfortunately, as it was embedded in the major phase, no information concerning its symmetry could be obtained. The monoclinic and tetragonal phases have not been isolated by TEM.

To summarize, after calcination at 1000 °C, three different phases coexist: phase 1: expected *I*4/*m* phase with expected composition; phase 2: *I*2/*m* Ba-free composition; phase 3: Cs-free composition. After sintering at 1200 °C, the only phase is *I*4/*m* phase with the expected composition (Scheme 2). As previously mentioned, because of large voids in the *I*2/*m* Ba-free phase (phase 2), Cs might be easily removed. The reaction mechanism during sintering at 1200 °C could be a solid reaction between phases 3 and 2 because of Cs mobility in the latter to form the expected *I*4/*m* product and complete its percentage from 75% (phase 1) to 100%.

Table 7
Interatomic Ba–O and Cs–O distances in tetragonal and monoclinic $Ba_1Cs_{0.28}Fe_{0.82}Al_{1.46}Ti_{5.72}O_{16}$ hollandite

Distances (Å)	Tetragonal hollandite		Distances (Å)	Monoclinic hollandite
Atoms	Ba	Cs	Atoms	Cs
O1	2.841(6)	2.723(8)	O1	3.09(5)
O1	3.075(6)	3.255(13)	O1	3.52(4)
O2	3.366(3)	3.401(4)	O2	3.04(4)
			O2	3.47(3)
			O3	3.32(6)
			O4	3.43(2)

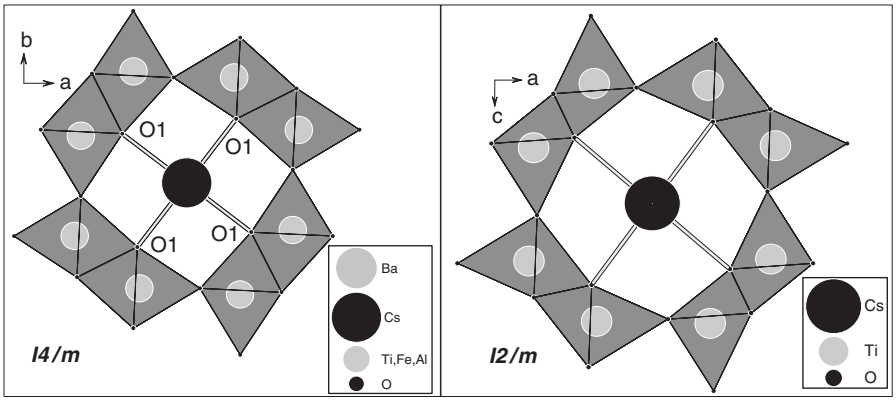

Fig. 9. Structure representation of tetragonal and monoclinic hollandite along the tunnel.

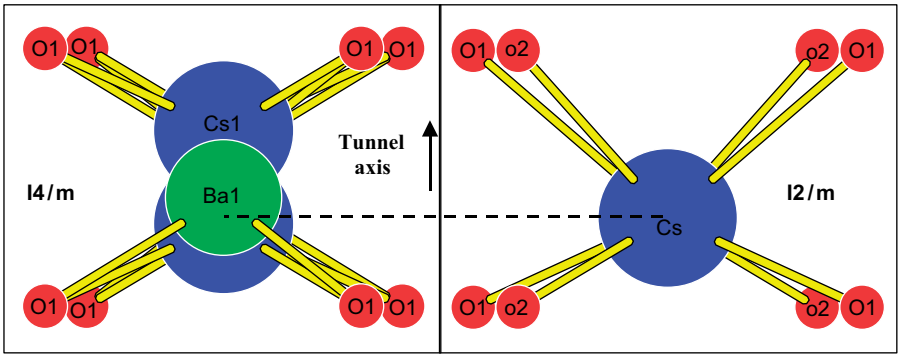

Fig. 10. Comparison of cesium and barium positions in the tetragonal and monoclinic prefired hollandite perpendicular to the tunnel axis.

4. Conclusion

To synthesize the $Ba_1Cs_{0.28}Fe_{0.82}Al_{1.46}Ti_{5.72}O_{16}$ hollandite, two different routes have been studied. The alcoxyde route is adapted only for large quantities. The dry one is used for low quantity but can be extrapolated to large amounts. In these two routes, same steps are used: calcination at 1000 °C and sintering at 1200 °C.

After sintering, the different synthesis routes are equivalent and give tetragonal hollandite (space group $I4/m$). Thanks to XRD patterns obtained at barium and cesium K absorption edges, two different positions for these two elements have been found: Ba is more centered in the cubic oxygen site in the tunnel than cesium.

After the calcination, the different synthesis routes do not give same results. The hollandite obtained by the oxide route is tetragonal and contains Cs and Ba with cell parameters a little different from those after sintering. By alcoxyde route, three phases are present: a tetragonal phase containing Ba and Cs and corresponding to the expected phase, a monoclinic phase containing only Cs and a phase containing only Ba with a weak coherence length. During the sintering, the last two phases should react to give the expected tetragonal hollandite with Ba and Cs.

Moreover, the final $Ba_1Cs_{0.28}Fe_{0.82}Al_{1.46}Ti_{5.72}O_{16}$ hollandite has a low ionic conductivity proving that cesium, in this material, is not mobile, which is in good agreement with leaching tests.

Acknowledgments

The authors acknowledge Professor M. Danot and Professor G. Ouvrard for Mössbauer experiments and XANES experiments, respectively.

References

[1] Law no. 91-1381, December 30, 1991, France.
[2] D.R. Lide, Handbook of Chemistry and Physics, CRC Press, Boca Raton, FL, USA, 1992–1993.
[3] R.J.W. Lugtenberg, Z. Brzozka, A. Casnati, R. Ungaro, J.F.J. Engbersen, D.N. Reinhoudt, Anal. Chim. Acta 310 (1995) 263.
[4] S.E. Kesson, Radioact. Waste Manage. Nucl. Fuel Cycle 4 (1983) 53.
[5] A.E. Ringwood, V.M. Oversby, S.E. Kesson, W. Sinclair, N. Ware, W. Hibberson, A. Major, Nucl. Chem. Waste Manage. 2 (1981) 287.
[6] S.E. Kesson, T.J. White, Proc. R. Soc. London A 405 (1986) 73.
[7] A. Byström, A.M. Byström, Acta Crystallogr. 3 (1950) 146.
[8] R.W. Cheary, Acta Crystallogr. B 42 (1986) 229.
[9] D.S. Filimonov, Z.-K. Liu, C.A. Randall, Mater. Res. Bull. 37 (2002) 2373.
[10] G. Leturcq, F. Bart, A. Comte, Patent No. EN: 01/15972, France, 2001.
[11] V. Petricek, M. Dusek, The Crystallographic Computing System JANA2000, Institute of Physics, Praha, Czech Republic, 2000.
[12] J. Rodriguez-Carvajal, Physica B 192 (1993) 55.
[13] B.A. HUNTER, Version 1.7.7, 1997.
[14] A. Albinati, et al., International Tables for Crystallography, Klumer Academic Publichers, Dordrecht/Boston/London, 1992.
[15] G. Evans, R.F. Pettifer, J. Appl. Crystallogr. 34 (2001) 82.
[16] P. Thompson, D.E. Cox, J.B. Hastings, J. Appl. Crystallogr. 20 (1987) 79–83.
[17] V.I. Goldanski, E.F. Makarov, V.V. Khrapov, Phys. Lett. 3 (1963) 344;
S.V. Kariagin, Dokl. Akad. Nauk SSSR 148 (1963) 1102.
[18] A.Y. Leinekugel-Le-Cocq-Errien, P. Deniard, S. Jobic, E. Gautier, M. Evain, V. Aubin, F. Bart, J. Solid State Chem., submitted for publication.
[19] R.W. Cheary, Mater. Sci. Forum 27/28 (1988) 397.
[20] S. Barbato, J.L. Gautier, Electrochim. Acta 46 (2001) 2767.
[21] H.P. Weber, H. Schulz, J. Chem. Phys. 85 (1986) 475.
[22] C. Fillet, T. Advocat, F. Bart, G. Leturcq, H. Rabiller, C. R. Chim. 7 (2004) 1165.
[23] J.-F. Bérar, P. Lelann, J. Appl. Crystallogr. 24 (1991) 1.
[24] R.W. Cheary, Acta Crystallogr. B 47 (1991) 325.
[25] R.D. Shannon, Acta Crystallogr. A 32 (1976) 751.